Polar Biol (2009) 32:443–452
DOI 10.1007/s00300-008-0538-5

ORIGINAL PAPER

Cumulative solar irradiance and potential large-scale sea ice algae distribution off East Antarctica (30°E–150°E)

Ben Raymond · K. Meiners · C. W. Fowler · B. Pasquer · G. D. Williams · S. Nicol

Received: 11 July 2008 / Revised: 16 October 2008 / Accepted: 28 October 2008 / Published online: 27 November 2008

Abstract We present a computational model of the large-scale cumulative light exposure of sea ice in the Southern Ocean off East Antarctica (30°E–150°E). The model uses remotely sensed or modelled sea ice concentration, snow depth over sea ice, and solar irradiance data, and tracks sea ice motion over the season of interest in order to calculate the cumulative exposure of the ice field to photosynthetically active radiation (PAR). Light is the limiting factor to sea ice algal growth over winter and early spring, and so the results have implications for the estimation of algal biomass in East Antarctica. The model results indicate that highly light-exposed ice is restricted to within a few degrees of the coast in the eastern part of the study region, but extends much further north in the 30°E–100°E sector. The relative influences of sea ice motion, solar flux, and snow depth variations on interannual variations in model predictions were evaluated. The model estimates of cumulative PAR were found to correlate with satellite estimates of subsequent open-water chlorophyll-*a* concentration, consistent with the notion that sea ice algae can provide inocula for phytoplankton blooms.

Keywords Sea ice · Sea ice motion · Photosynthetically active radiation · Sea ice algae · East Antarctica

B. Raymond (✉) · S. Nicol
Australian Antarctic Division, Channel Highway, Kingston, TAS 7050, Australia
e-mail: ben.raymond@aad.gov.au

B. Raymond · K. Meiners · B. Pasquer · G. D. Williams · S. Nicol
Antarctic Climate and Ecosystems Cooperative Research Centre, Private Bag 80, Hobart, TAS 7001, Australia

C. W. Fowler
Colorado Center for Astrodynamics Research, Aerospace Engineering Sciences Department, University of Colorado, Boulder, CO 80309-0431, USA

G. D. Williams
Institute for Low Temperature Science, Hokkaido University, Sapporo 060-0819, Japan

Introduction

Sea ice is an important structuring element of the Southern Ocean ranging in area between 4 million km^2 in February and 19 million km^2 in September (Gloersen et al. 1992; Thomas and Dieckmann 2003). The sea ice cover provides a vast habitat for ice-associated algae, which form distinct communities at the snow–ice interface, and in the interior and at the base of sea ice floes (Ackley and Sullivan 1994; Gradinger 2002; Arrigo 2003). Sea ice algae contribute significantly to the overall ecosystem primary production (Legendre et al. 1992; Arrigo et al. 1997; Lizotte 2001; Arrigo and Thomas 2004) and provide a crucial, highly concentrated food source for pelagic grazers during winter and early spring when water column production is low. Juvenile krill, for example, have been observed feeding at the underside of sea ice (Stretch et al. 1988) and it has been shown that in the Antarctic Peninsula region there is a correlation between the extent of winter sea ice and the subsequent recruitment of krill (Siegel and Loeb 1995; Hewitt 2003; Siegel 2005). In the region of East Antarctica between 80°E and 150°E, sea ice extent is associated with biological activity at all trophic levels (Nicol et al. 2000).

Sea ice algae data are derived mainly from coring surveys, and are still very sparse in the East Antarctic region.

Consequently, the large-scale distribution of sea ice algae off East Antarctica, and the influences of physical factors such as the timing and location of ice formation, ice drift, snow thickness and the exposure of ice floes to photosynthetically active radiation (PAR) on that distribution, are still poorly understood.

Arrigo et al. (1997) developed the first quantitative sea ice primary production model for the Southern Ocean. Their model uses a radiative transfer model and also includes nutrient availability which is coupled to the flooding of sea ice floes. Based on sea ice ecological observations in the Weddell Sea the model primarily focuses on the development of internal and surface communities and neglects bottom communities (Arrigo et al. 1997). Subsequent model developments were carried out by Fritsen et al. (1998) and Belém (2002), both also focussing on Weddell Sea ice physical and biological properties. Recent observations off East Antarctica show that ice algal biomass in this area is mainly restricted to bottom ice layers (Grose and McMinn 2003; McMinn et al. 2007) and thus these models may be not appropriate for this sector of the Southern Ocean. In comparison to many other areas of the sea ice zone, East Antarctica has a short pack ice season and low snow accumulation and therefore may be less likely to develop surface algal communities caused by snow-loading and flooding (Fritsen et al. 1994; McMinn et al. 2007).

As a first step towards a sea ice algae model for East Antarctica, we present a relatively simple model to explore the spatial and temporal patterns of light exposure of sea ice off East Antarctica. Belém (2002) varied the physical forcing parameters of his model (e.g. air temperature and solar flux) according to the time-dependent position of ice floes, calculated from sea ice velocity fields. We adopted a similar approach here and used ice drift, solar irradiance, and snow depth data to estimate the cumulative PAR exposure of ice floes. Under the assumption that light is the limiting factor for the growth of ice algae over the winter period, particularly for bottom communities, our model has implications for the spatial distribution of standing stock in East Antarctic sea ice.

Methods

Our model aimed to estimate the light regime experienced across the sea ice field, based on the movement and formation dynamics of the sea ice and the available light. The model was run on a 1° grid covering the region from 55°S to 70°S and 30°E to 150°E (Fig. 1). A 1° grid spacing corresponds to a latitudinal distance of ~110 km, and a longitudinal distance of ~50 km at 62.5°S. Results were computed for 1979–2004, from the first of March to the first of November; approximately the austral autumn to early spring period.

The average daily solar radiation was tabulated for each day of the season of interest, using bilinear interpolation of NCEP/NCAR surface-level downward solar radiation flux (Wm^{-2}; daily, 2° resolution) (Kalnay et al. 1996). We estimated the photosynthetically active component of this flux (PAR) as 0.48 of the total flux (Frouin and Pinker 1995). This PAR is incident on the surface of the snow which lies over the sea ice (or on the surface of the ice if no snow is present). A proportion of this radiation is reflected by the snow (or ice) surface, with the proportion determined by the surface albedo. Brandt et al. (2005) reported visible-band albedos of 0.11–0.96 for various types of ice and depths of snow cover in the East Antarctic region. Our model does not differentiate between ice types, and so we assumed a representative albedo value of 0.75. Thus, the PAR just beneath the surface is 0.25 of the incident PAR. The attenuation of PAR through the snow layer was modelled as an exponential decrease with snow depth (Beer's law):

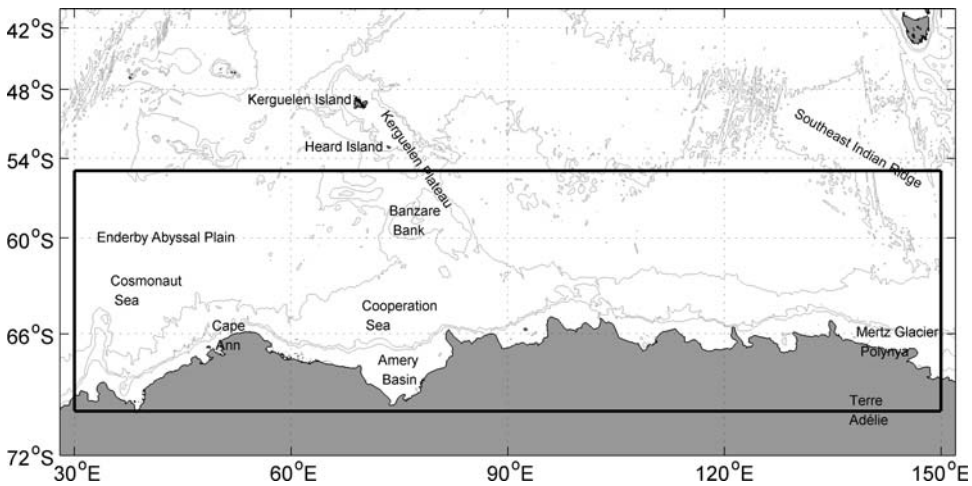

Fig. 1 The study area off East Antarctica

$$\mathrm{PAR}(z) = \mathrm{PAR}_0 e^{-\kappa z},$$

where PAR_0 is the PAR just below the snow surface, z is the depth of the snow layer, and κ is the extinction coefficient. A value of 14 m^{-1} was used for the extinction coefficient (Lavoie et al. 2005). The depth of this snow layer was taken from SMMR-SSM/I data (depth in metres; daily, 25 km resolution) (Markus and Cavalieri 2006). The attenuation of PAR through the sea ice itself was not modelled, as we did not have appropriate sea ice thickness data available. The calculated PAR at a given point thus corresponds to the light reaching the surface (not the underside) of the sea ice at that point.

We calculated the movement of the sea ice field across the season, using the 1° grid points as the final positions of interest and working backwards in time. For each day of the season, the sea ice motion (Fowler 2003) at each grid point location was used to back-calculate the position of that point on the previous day, in a similar manner to the drift simulation calculations used by Belém (2002). Sea ice motion was derived from buoy and satellite data (Fowler 2003), with daily coverage and spatial resolution of ~25 km. From the calculated positions of each grid point in geographic space over the season of interest, the daily values of the sea ice concentration (SMMR-SSM/I percentage cover; daily, 25 km resolution) (Cavalieri et al. 1996, updated 2006), snow depth, and PAR were collated. The dates of ice formation and melt were calculated for each grid point, using 15% concentration as the threshold at which the ice was considered to have melted or formed. The cumulative PAR exposure of each point in the model grid was then calculated by summing the PAR values between those dates. In many cases there were multiple formation and melt sequences for a single grid point. In such cases, the cumulative PAR was summed over all periods for which ice was present (>15% concentration).

Temporal and spatial variations in snow cover, ice motion, and solar irradiance have varying temporal and spatial effects on the model estimates. The partial effects of variations in snow cover were investigated by re-running the model with a constant snow depth of 7.9 cm. This depth was calculated to give a long-term mean cumulative PAR equal to that obtained by the full model. The results obtained from the constant snow depth model were subtracted from the full model results to show the relative effects of snow cover variations over space and season. A similar approach was used to evaluate the partial effects of sea ice motion and solar flux variations, using models with constant zero sea ice motion and constant PAR flux level (77.7 $\mathrm{W/m}^2$; again calculated to give a long-term mean cumulative PAR equal to that obtained by the full model). The partial effects of snow cover, ice motion, and solar flux variations were averaged over the 1979–2004 seasons. The relative sizes of the absolute values of those mean partial effects were then compared to establish the relative influences of these three factors on interannual variations in cumulative PAR.

The model is intended to estimate cumulative light exposure, in the context of potential ice algal growth under light-limited conditions. These estimates should ideally be compared with measurements of algae, for example obtained from sea ice cores. However, we were able to find only 89 records of algal biomass from first-year ice cores collected between 15 October and 31 November in our study area. These data were obtained from published literature (Watanabe et al. 1990; Swadling 2001; Trevena and Jones 2006; McMinn et al. 2007) and from files held by the Australian Antarctic Data Centre (http://data.aad.gov.au/). Of these 89 records, 44 were from coastal sites, where our results may be unreliable (see Sect. "Discussion"). Thirty-six of the remaining 45 were concentrated in two relatively small areas between 106°E–111°E, and 146°E–148°E, and all were located south of 63.5°S. This number and distribution of cores is inadequate to allow meaningful comparison with the outputs from our model. Model outputs were instead compared with remotely sensed estimates of open-water surface chlorophyll-*a* obtained from SeaWiFS satellite data. There is a widely held view that sea ice algae provide inocula for phytoplankton blooms after sea ice melt (Smith Jr and Nelson 1985; Garrison et al. 1987; Lizotte 2001) and so areas of sea ice with high standing stock of ice algae might be expected to show higher subsequent concentrations of open-water phytoplankton. In examining the correlation with open-water chlorophyll-*a*, grid points on ice that did not melt during the season of interest were excluded. Chlorophyll-*a* concentrations were calculated as 1997–2004 November means in 1° cells, to match the model grid; missing SeaWiFS data due to cloud cover were excluded from the averages.

Results

The long-term average cumulative PAR values are shown in Fig. 2a and ranged from 165 to 635 W days m^{-2} (5th to 95th percentile). Averaged over the 246 days of the study period, these equate to mean daily PAR values of 0.68–2.58 Wm^{-2}. The long-term average spatial distribution of cumulative PAR is shown in Fig. 2a. In the sector from 100°E to 150°E, the areas of maximum cumulative PAR (greater than ~550 W days m^{-2}) were patchy and generally limited to within a few degrees of latitude of the coast, but in the sector from 60°E to 100°E similar areas extended much further north, out to ~59°S over the Kerguelen Plateau, at ~80°E. The sector from 30°E to 60°E showed moderate levels of cumulative PAR, with the highest

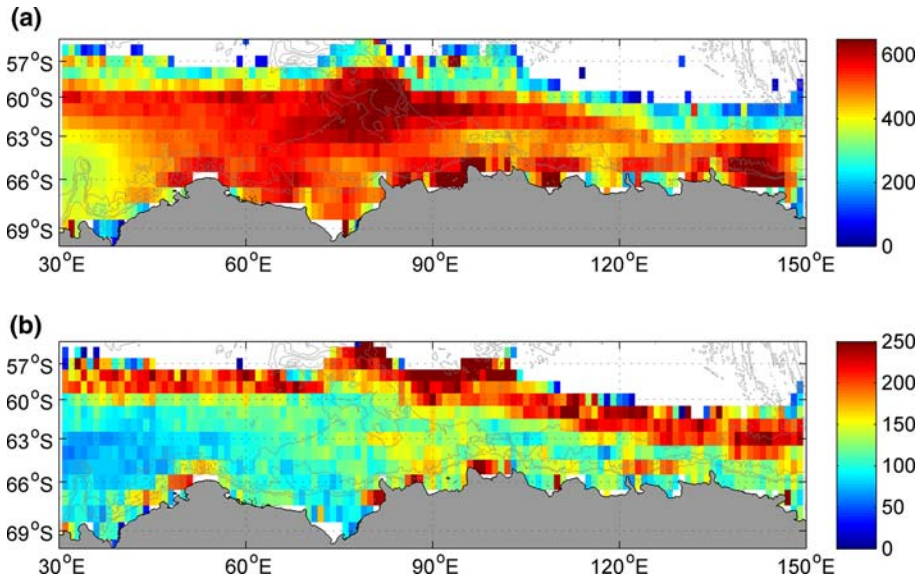

Fig. 2 Estimated cumulative PAR exposure of sea ice in East Antarctica. **a** Mean, and **b** SD across the 1979–2004 autumn–spring seasons. Units are W days m^{-2}

values around Cape Ann (~50°E) and in an offshore band at ~60°S. The lower values (~375 W days m^{-2}) off the coast of the 30°E–40°E sector correspond to the location of the Cosmonaut Sea embayment (Geddes and Moore 2007). The interannual variation of cumulative PAR (Fig. 2b) was lowest in the 30°E–50°E sector, and highest in patches along the coast and along the seaward margin of the pack.

The age at melt was calculated for the ice in each grid cell from the dates of formation and melt. The estimated cumulative PAR is shown against the age at melt in Fig. 3a. This figure shows that the highest levels of cumulative PAR occurred in the oldest ice, as one might expect. However, the fitted curve also shows a broad intermediate peak, indicating that elevated cumulative PAR levels were also associated with ice of moderate age (~40–150 days old). Figure 3b shows the spatial distribution of ice with cumulative PAR of >750 W days m^{-2}. The differences in the distributions of the two age classes are clear: elevated cumulative PAR in the oldest ice (>200 days) was distributed along the coast, and reached further offshore over the Kerguelen Plateau and in the 130°E–150°E sector. Elevated cumulative PAR values in younger ice were distributed towards the northern margin of the ice pack, particularly in the 30°E–120°E sector.

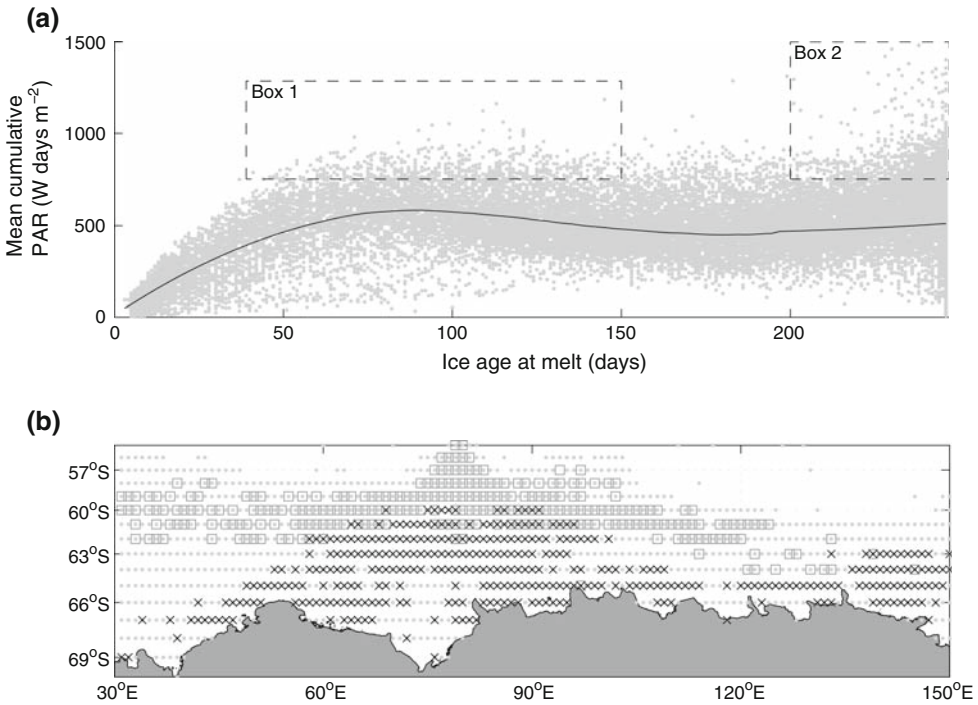

Fig. 3 **a** Estimated cumulative PAR and the age at melt of the ice. *Each point* represents a single grid point at the end of a single season. *Grey points* show data from all 26 seasons of the model; *black line* shows smooth (loess) fit. *Points within Box 1* (relatively high cumulative PAR in relatively young ice) are shown as *squares* in **b**; *points within Box 2* (relatively high cumulative PAR in relatively old ice) are shown as *crosses* in **b**. **b** The spatial distribution of the *points* in **a**

Figure 4a shows the spatial and temporal variations in the effects of sea ice motion. The values shown in the figure are the differences between model estimates using no sea ice motion, and those of the full model. Positive values indicate that the inclusion of motion causes an increase in the model estimate of cumulative PAR, and this can be seen to be true particularly in the 60°E–90°E sector and off Terre Adélie (130°E–150°E). Few sectors showed consistent decreases in cumulative PAR estimates with the inclusion of ice motion effects: only the 30°E–40°E and 110°E–120°E sectors showed relatively consistent negative values (Fig. 4a). The effects of ice motion were minimal prior to 1982, although this might be attributable to methodological problems (see Sect. "Discussion").

Figure 4b shows the effects of spatial and temporal variations in the depth of snow on the surface of the sea ice. Similarly to Fig. 4a, the values shown are the differences between model estimates using a fixed, constant snow depth, and those of the full model, and positive values indicate that the inclusion of snow variations causes an increase in the model estimate of cumulative PAR. The inclusion of snow variations in the model caused fairly consistent decreases in the estimates of cumulative PAR (negative values in Fig. 4b) in the 30°E–40°E sector. Snow effects were also generally negative in the 140°E–150°E sector, particularly from about 1992. The remainder of the study area showed generally positive snow effects (i.e. increases in cumulative PAR estimates with the inclusion of snow variations in the model) up to about 1998, and mixed effects thereafter.

Spatial and temporal variations in solar flux caused positive effects (i.e. an increase in the estimated cumulative PAR with flux variations included) in the 40°E–90°E sector, particularly from about 1989 (Fig. 4c). The 90°E–150°E sector showed generally negative effects.

The interannual variations in cumulative PAR between 30°E and 60°E were most strongly affected by variations in downward PAR flux (green colour component; Fig. 5) and snow cover (blue). Snow cover also tended to control the interannual variation along the coast and in offshore pack ice. Ice motion (red) affected interannual variability in the inner and mid pack between 60°E and 90°E and off Terre Adélie (~140°E).

The mean November chlorophyll-*a* derived from SeaWiFS satellite data (1997–2004) showed broadly similar patterns to the 1997–2004 mean model estimate of cumulative PAR (Fig. 6). The mean cumulative PAR estimates in this figure were calculated only from pixels that had melted by the ending date of each model run (i.e. by 1 November each season). These pixels spanned a band of ice extending across about 3–4° of latitude (~330–440 km) at the northernmost extent of the ice pack, located

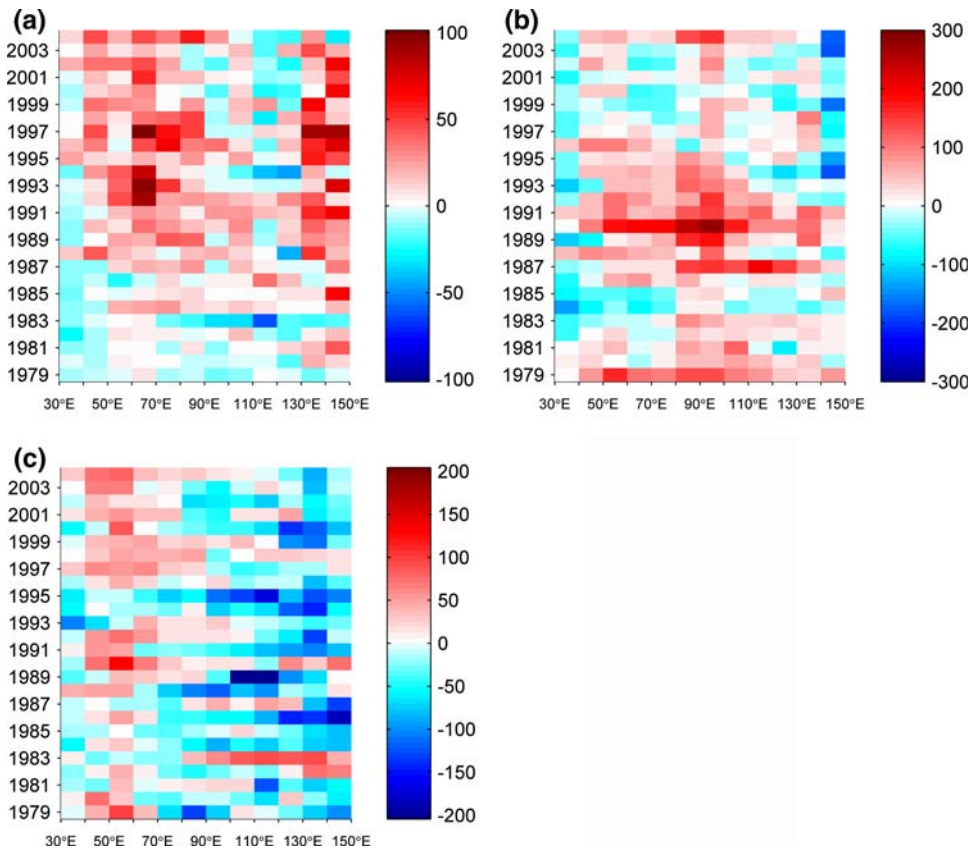

Fig. 4 Spatial and temporal variations in the effects of **a** ice motion, **b** snow depth, **c** solar flux. Values are the differences between a model with **a** no ice motion, **b** fixed, constant snow depth, or **c** fixed, constant flux, and those of the full model. *Positive values* indicate that the inclusion of the parameter in question causes an increase on the model estimate of cumulative PAR. All values in W days m^{-2}

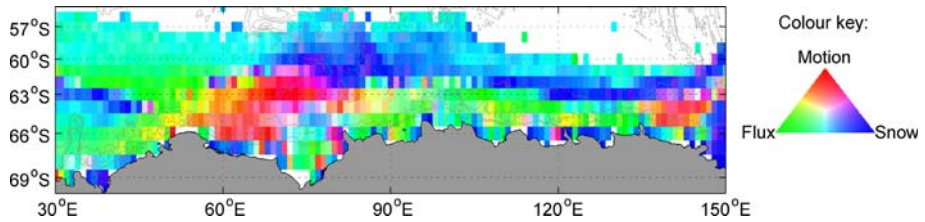

Fig. 5 The spatial pattern of the drivers of interannual variations in modelled cumulative PAR. The *red*, *green*, and *blue colour* components of each grid cell represent the relative contributions from ice motion, solar flux, and snow depth variations

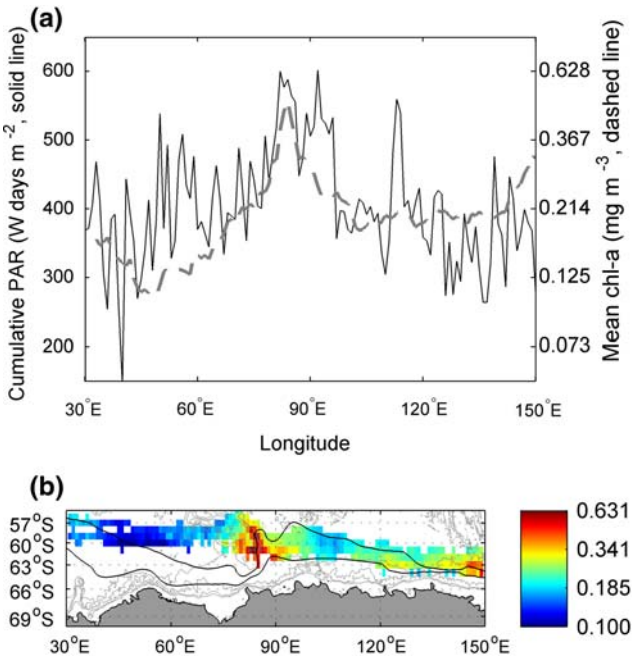

Fig. 6 **a** 1997–2004 Mean November SeaWiFS chlorophyll-*a* (*dashed line*) and cumulative PAR (*solid line*), in 1° longitude sectors. **b** 1997–2004 Mean November SeaWiFS chlorophyll-*a* distribution. The *solid lines* show the positions of the southern Antarctic Circumpolar Current front (*upper line*) and the southern boundary of the Antarctic Circumpolar Current (*lower*; front positions from Orsi et al. 1995)

at about 59°S at 30°E and at about 63°S at 150°E (Fig. 6b). The longitudinal distributions of the two signals show broad similarities, with low values in the west, rising to maxima around 85°E and moderate values in the east (Fig. 6a). The Spearman rank correlation between cumulative PAR estimates from the full model and the SeaWiFS chlorophyll-*a* was moderate but significant ($r_s = 0.34$, $P < 0.02$; $N = 121$). Using cumulative PAR estimates from the model run with constant snow depth improved this correlation to $r_s = 0.67$ ($P < 0.01$; $N = 121$).

Discussion

We have presented a simple model for the cumulative light exposure of sea ice off East Antarctica and explored the impact of ice drift, snow cover and downward solar flux on model outputs. The modelled light exposure distribution correlates with SeaWiFS-derived surface chlorophyll-*a* concentrations in the marginal ice zone following ice melt. This comparison is at best a weak validation of the model, due primarily to the fact that our model provides estimates of light exposure, rather than specifically of algal biomass, and also due to the number of processes that can affect the chain of events between the release of ice algae into the water column and any subsequent phytoplankton bloom. A more rigorous validation of the model will be possible once more extensive sea ice core data become available.

The current model is deliberately simplistic, focussing on light availability over the winter–spring period and first-year ice only. The effects of snow cover are restricted to the attenuation of light as it passes through the snow layer, and this effect is parameterised by an exponential decrease with snow depth, with no differential attenuation by wavelength or according to the physical structure of the snow. The depth of snow cover may be underestimated: passive microwave estimates of snow depth have been shown to underestimate in situ measurements (Markus and Cavalieri 1998; Worby et al. 2008b). Snow cover plays a key role in flooding of sea ice and subsequent thermodynamic thickening of the sea ice from above by snow ice formation, which strongly affects optical properties of the sea ice (Worby et al. 1998). Flooding also causes the formation of infiltration communities, which add to the integrated sea ice primary production, and also attenuate the light reaching the bottom of the sea ice, an effect known as "self-shading" (Palmisano et al. 1987). Previous work has shown that most algal biomass is located in the bottom few centimetres in ice core samples off East Antarctica (McMinn et al. 2007). Consequently, the importances of these effects in models developed for this region are uncertain. Light reaching the bottom of the sea ice would be further attenuated by the ice itself. Our model has no ice thickness component (vertical dimension) as currently there are no reliable ice thickness estimates available at a sufficiently broad scale to match the remainder of the model inputs. Sea ice thicknesses in the range 0.35–0.72 m (Allison et al. 1993; Worby et al. 2008a) and mean snow cover depths in the range 0.05–

0.15 m (Massom et al. 2001) have been reported for the East Antarctic sector. Although the attenuating effect of ice is approximately an order of magnitude less than that of snow (Perovich 1996), these values suggest that the attenuation of light within the ice may be comparable to that in the overlying snow, and will need to be considered in future model developments. Nutrient availability will be critically important for future model development covering the summer months, when light ceases to be a limiting factor.

The model results close to the coast are unlikely to be reliable, due to both the inaccuracy of sea ice motion data close to the coast (Fowler 2003), and the relative coarseness of the 1° model grid with respect to variations in the geometry of the coast. Even in open ocean regions, satellite-derived sea ice motion data has been shown to underestimate the true sea ice motion by up to 40% when compared to buoy measurements (Heil et al. 2001). Thus the effects of sea ice motion may be underestimated in our model, particularly in those sectors where we found motion to have a large effect (60°E–90°E and 140°E–150°E). Underestimation of ice motion is particularly problematic during spring melt, because the model will effectively assume that sea ice melted in a given grid cell, whereas in fact the ice was removed by advection, with less local release of fresh water and sea ice algae inocula into the water column (Fitch and Moore 2007). The effects of ice motion in the model were minimal for the earliest seasons (1979–1981). The ice motion estimates prior to 1982 were based principally on SMMR data (with a spatial resolution of 25 km), as AVHRR data (spatial resolution 5 km) were available only from 1982 onwards and SSM/I (spatial resolution 12.5 km) from 1988 onwards (Fowler 2003). The reduced effect of sea ice motion in the model prior to 1982 may thus be an artefact of the coarser spatial resolution in the sea ice data used to estimate the ice motion during this period. Other dynamic effects such as wave–ice interaction at the seaward margin of the ice pack, and rapid opening and closing of the pack in storm events, were not modelled.

High values of cumulative PAR in our model estimates were generally restricted to coastal regions, except in the 60°E–100°E sector where high values extended northwards over the Kerguelen Plateau (Fig. 2a). This sector shows northward winter sea ice motion (Heil and Allison 1999), thus providing an offshore transport of coastal ice [Fig. 7; see also Rintoul et al. (2008) for an overview of sea ice dynamics in the 80°E–90°E sector]. This pattern matches that reported by Garrison et al. (2003), who found high biomass in offshore ice and low biomass in more inshore ice in the Ross Sea, and concluded that the northward export of older sea ice is responsible for this pattern of the large-scale ice algal distribution in the Ross Sea.

Arrigo et al. (2003) reported a bimodal distribution of spring ice algal biomass along a transect through the Ross Sea pack ice with a minimum ice algal biomass usually found in young sea ice and sea ice with a heavy snow cover. The authors explained the overall latitudinal distribution of ice algal biomass in terms of ice thickness, age and snow thickness as well as heterotrophic activity. McMinn et al. (2007), studying sea ice in the same area as our study, found a positive correlation of integrated sea ice algal biomass and ice thickness but no relationship between sea ice algal biomass and latitude of sampling site. This is in agreement with our model, which shows that the cumulative PAR distribution does not follow a simple zonal pattern. Generally, our model found elevated cumulative PAR in two situations: old ice, which tended to be coastally distributed but transported further north in some sectors (notably 60°E–90°E), and also younger ice, formed later in the season and found towards the northern extent of the pack.

The inclusion of snow variations in the model caused decreases in the estimates of cumulative PAR in the 30°E–40°E and 140°E–150°E sectors, suggesting that these sectors accumulate greater than the regional average snow depth. This reflects the observed snow depths: the East Antarctic sector from about 40°E to 145°E displays lower mean September snow depths than the remainder of the Antarctic (Markus and Cavalieri 2006). The inclusion of snow variations caused decreases in the cumulative PAR estimates across the study entire region from about 1998 (a mean decrease of 5.6% relative to pre-1998 levels; Fig. 4b), broadly matching the observed increase in Antarctic-wide September snow depths from about 1999 (Markus and Cavalieri 2006).

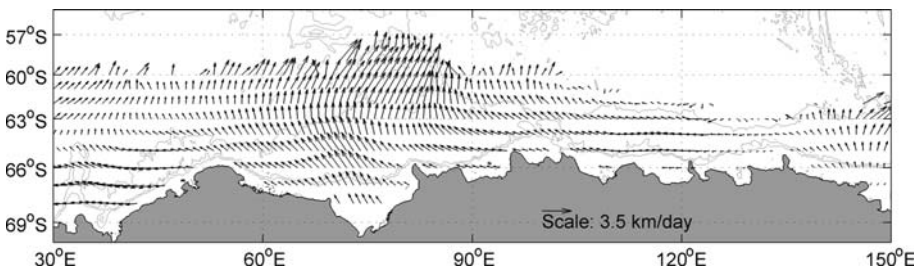

Fig. 7 Mean August sea ice motion in the study area, derived from buoy and satellite data (adapted from Fowler 2003)

McMinn et al. (2007) reported photoadaptive index (E_k) values of 19–44 μmol photons m^{-2} s^{-1} in East Antarctic sea ice algae sampled in spring. At light levels below the photoadaptive index, growth is light-limited. These values can be converted to irradiances in Wm^{-2} using the equation:

$$F = E_k hcN_A/\lambda \times 10^{-6},$$

where F is the flux in Wm^{-2}, h is Planck's constant, c is the speed of light, N_A is the Avogadro constant, and λ is the wavelength of the light. Using a mean wavelength of 550 nm for PAR, this range of E_k values equates to irradiances of 4.1–9.6 Wm^{-2}. These values are slightly higher than the long-term mean daily PAR values shown in Fig. 2a (0.68–2.58 Wm^{-2}).

We are aware of only one published estimate of the regional spatial distribution of sea ice algae in East Antarctica (Grose and McMinn 2003). This estimate was based on ice cores and shipboard observations from 103°E–110°E, and extrapolated to the wider East Antarctic region based on ice type and snow thickness estimates obtained from passive microwave images. The biomass distribution for November of 2000 in Figure 3 of Grose and McMinn (2003) shows the highest biomass in the inner pack from about 30°E to 75°E, and in patchy areas along the coast eastwards to 150°E. This pattern is broadly similar to the long-term mean cumulative PAR shown in our Fig. 2a, except that highly light-exposed ice extends much further offshore in the 60°E–90°E sector, and the inshore area from 30°E to 50°E accumulates only moderate PAR. The 60°E–90°E sector exhibits pronounced northward winter sea ice motion (Fig. 7), and the inshore 30°E–50°E sector displays highly variable sea ice conditions (Geddes and Moore 2007), suggesting that the effects of sea ice dynamics could be an important consideration in the estimation of algal biomass.

Based on microscopic analysis of the species composition in sea ice and associated pelagic blooms, seeding has been suggested for different parts of Antarctic marginal ice zone [see e.g. Arrigo et al. (2003) for a summary]. Plumes of particulate organic matter and algae released from sea ice have been observed and can increase phytoplankton biomass at ice edges (Wright and van den Enden 2000). Such seeding and the development of ice-edge blooms is not ubiquitous, but is dependent on others factors that affect sedimentation and growth rates of algae at the ice edge. Important factors, among others, include the retreat rate of the sea ice, wind stress, current regime, interactions with bathymetry, iron release due to melting, ice algal species composition and their potential for aggregation, as well as the occurrence of herbivores (Smith Jr and Nelson 1985; Lancelot et al. 1993; Sedwick and DiTullio 1997; Fitch and Moore 2007; Lannuzel et al. 2007). Our results indicate a correlation between cumulative PAR and subsequent ice edge bloom strength, consistent with the seeding hypothesis. This interpretation is confounded to some extent by the fact that ice with high cumulative PAR tends to be older and therefore thicker, yielding a greater release of fresh water and potentially iron on melt, both of which would tend to favour subsequent blooms, from either algae seeded from the melted ice, or from pelagic phytoplankton already in the surface waters.

The correlation with open-water chlorophyll-*a* concentration was stronger for the model with constant snow depth ($r_s = 0.67$) than the full model ($r_s = 0.34$); however, this improvement in correlation is likely to be a simple reflection of the fact that the constant snow depth estimates of cumulative PAR were less noisy (displayed less small-scale longitudinal variation). Both models tended to consistently overestimate chlorophyll-*a* in the 50°E–90°E sector and underestimate in the 90°E–140°E sector. This longitudinal pattern in the residuals possibly indicates longitudinal differences in the processes that complete the chain of events from spring ice retreat to subsequent open-water bloom. There are obvious longitudinal differences in bathymetry and ocean currents: the band of interest in the 50°E–90°E sector (at ~60°S; Fig. 6b) lies immediately to the east of the deep water of the Enderby Abyssal Plain (~5,000 m), and north of the southern Antarctic Circumpolar Current front (SACCF); in the 90°E–140°E sector the band of interest lies closer to the shore over shallower water, and is congruent with the SACCF. These differences alone are likely to influence factors such as nutrient supply to potential blooms (Constable et al. 2003).

A common observation in the Southern Ocean is the increased frequency of phytoplankton blooms near the Antarctic coast, relative to offshore waters (e.g. Fitch and Moore 2007). This association with coastal regions is likely due to a number of factors, including iron availability due to both melting sea ice as well as mixing of iron-rich shelf sediments into the mixed layer (Fitch and Moore 2007), but nonetheless is in agreement with our observation of high accumulated PAR values in coastal sea ice. Nicol et al. (2000) showed that sea ice extent—controlled by ocean circulation—affects biological productivity at all trophic levels in the 80°E–150°E sector. They found high concentrations of krill to be restricted to coastal locations in the eastern side of this area, but extending further offshore (to ~63°S, the northernmost limit of their survey) west of 115°E. Our model outputs are consistent with these observations, with a similar spatial distribution of sea ice cumulative PAR in the same sector, but we note that the westward and northward winter sea ice motion in the west of this sector (80°E–115°E) would provide an offshore transport mechanism for krill larvae associated with the ice (Thorpe et al. 2007) and other biological material taken up

from coastal locations. The increased abundance of krill offshore in the 80°E–115°E sector might be due to offshore transport, active migration (Nicol 2006), or increased offshore sea ice algae availability, or a combination of these and other factors (Smith Jr and Comiso 2008).

Future Antarctic sea ice conditions under climate change scenarios are uncertain (Parkinson 2004), although regional changes in sea ice extent and season have already been reported for the southern hemisphere (Parkinson 2002; Zwally et al. 2002; Cavalieri and Parkinson 2008). A shortening of the sea ice season would result in decreased cumulative exposure of ice floes to PAR and thus potentially reduce sea ice primary production during winter when light is limiting ice algal growth. Global circulation models indicate a climate change driven increase in precipitation that may increase the sea ice snow cover, affecting sea ice growth and algal distribution (Watterson and Dix 2003; Powell et al. 2005; Monaghan et al. 2008). The direct effect of increased snow cover would be to reduce the light penetrating to the sea ice, but more complex effects would include increased snow ice formation, flooding of ice floes, and the development of surface and interior communities (Arrigo et al. 1997; Massom et al. 2001; Arrigo and Thomas 2004).

Our study underlines the important ecological role of sea ice in the Southern Ocean and provides a better understanding of the large-scale light exposure of sea ice. Further work is needed to understand physical–biological interactions in East Antarctic marine ecosystems by developing more advanced sea ice algal primary production models as well as medium-large scale sampling methodology to validate model outputs.

Acknowledgments Thorsten Markus provided the SMMR-SSM/I snow depth data. Comments from Delphine Lannuzel, Jan Lieser, and four anonymous reviewers greatly improved the manuscript. This research was supported by the Australian Government Cooperative Research Programme through the Antarctic Climate and Ecosystems Cooperative Research Centre (ACE CRC), and by the Australian Antarctic Division under AAS Project 2943.

References

Ackley SF, Sullivan CW (1994) Physical controls on the development and characteristics of Antarctic sea ice biological communities—a review and synthesis. Deep Sea Res Part I Oceanogr Res Pap 41:1583–1604

Allison I, Brandt RE, Warren SG (1993) East Antarctic sea ice: albedo, thickness distribution, and snow cover. J Geophys Res 98:12417–12429

Arrigo KR (2003) Primary production in sea ice. In: Thomas DN, Dieckmann GS (eds) Sea ice: an introduction to its physics, chemistry, biology and geology. Blackwell Scientific, Oxford, pp 143–183

Arrigo K, Thomas D (2004) Large scale implications of sea ice biology in the Southern Ocean. Antarct Sci 16:471–586

Arrigo KR, Worthen DL, Lizotte MP, Dixon P, Dieckmann G (1997) Primary production in Antarctic sea ice. Science 276:394–397

Arrigo KR, Robinson DH, Dunbar RB, Leventer AR, Lizotte MP (2003) Physical control of chlorophyll *a*, POC, and TPN distributions in the pack ice of the Ross Sea, Antarctica. J Geophys Res 108:3316. doi:3310.1029/2001JC001138

Belém AL (2002) Modeling physical and biological processes in Antarctic sea ice. Ph.D. thesis, Alfred Wegener Institute for Polar and Marine Research, Bremerhaven

Brandt RE, Warren SG, Worby AP, Grenfell TC (2005) Surface albedo of the Antarctic sea ice zone. J Clim 18:3606–3622

Cavalieri DJ, Parkinson CL (2008) Antarctic sea ice variability and trends, 1979–2006. J Geophys Res 113:C077004. doi:077010.071029/072007JC004564

Cavalieri D, Parkinson C, Gloersen P, Zwally HJ (1996, updated 2006) Sea ice concentrations from Nimbus-7 SMMR and DMSP SSM/I passive microwave data. National Snow and Ice Data Center, Boulder [digital media]

Constable AJ, Nicol S, Strutton PG (2003) Southern Ocean productivity in relation to spatial and temporal variation in the physical environment. J Geophys Res 108:8079. doi:8010.1029/2001JC001270

Fitch DT, Moore JK (2007) Wind speed influence on phytoplankton bloom dynamics in the Southern Ocean Marginal Ice Zone. J Geophys Res 112:C08006. doi:10.1029/2006JC004061

Fowler C (2003) Polar Pathfinder Daily 25 km EASE-Grid Sea Ice Motion Vectors. National Snow and Ice Data Center, Boulder [digital media]

Fritsen CH, Lytle VI, Ackley SF, Sullivan CW (1994) Autumn bloom of Antarctic pack-ice algae. Science 266:782–784

Fritsen CH, Ackley SF, Kremer JN, Sullivan CW (1998) Flood-freeze cycles and microalgal dynamics in Antarctic pack ice. In: Lizotte MP, Arrigo K (eds) Antarctic sea ice: biological processes, interactions and variability, vol 73. American Geophysical Union, Washington, DC, pp 1–21

Frouin R, Pinker RT (1995) Estimating photosynthetically active radiation (PAR) at the Earth's surface from satellite observations. Remote Sens Environ 51:98–107

Garrison DL, Buck KR, Fryxell GA (1987) Algal assemblages in Antarctic pack ice and in ice-edge plankton. J Phycol 23:564–572

Garrison DL, Jeffries MO, Gibson A, Coale SL, Neenan D, Fritsen C, Okolodkov YB, Gowing MM (2003) Development of sea ice microbial communities during autumn ice formation in the Ross Sea. Mar Ecol Prog Ser 259:1–15

Geddes JA, Moore GWK (2007) A climatology of sea ice embayments in the Cosmonaut Sea, Antarctica. Geophys Res Lett 34:L02505. doi:10.1029/2006GL027910

Gloersen P, Campbell WJ, Cavalieri DJ, Comiso JC, Parkinson CL, Zwally HJ (1992) Arctic and Antarctic sea ice, 1978–1987: satellite passive microwave observations and analysis. NASA Special Publications. National Aeronautics and Space Administration, Washington, DC

Gradinger R (2002) Sea ice microorganisms. In: Bitton G (ed) The encyclopedia of environmental microbiology. Wiley, New York, pp 2833–2844

Grose M, McMinn A (2003) Algal biomass in east Antarctic pack ice: how much is in the east? In: Huiskes AHL, Gieskes WWC, Rozema J, Schorno RML, van der Vies SM, Wolff WJ (eds) Antarctic biology in a global context. Proceedings of the VIIIth SCAR international biology symposium. Backhuys Publishers, Leiden

Heil P, Allison I (1999) The pattern and variability of Antarctic sea-ice drift in the Indian Ocean and western Pacific sectors. J Geophys Res 104:15789–15802

Heil P, Fowler CW, Maslanik JA, Emery WJ, Allison I (2001) A comparison of East Antarctic sea-ice motion derived using drifting buoys and remote sensing. Ann Glaciol 33:139–144

Hewitt RP (2003) An 8-year cycle in krill biomass density inferred from acoustic surveys conducted in the vicinity of the South Shetland Islands during the austral summers of 1991–1992 through 2001–2002. Aquat Living Resour 16:205–213

Kalnay E, Kanamitsu M, Kistler R, Collins W, Deaven D, Gandin L, Iredell M, Saha S, White G, Woollen J, Zhu Y, Leetmaa A, Reynolds B, Chelliah M, Ebisuzaki W, Higgins W, Janowiak J, Mo K, Ropelewski C, Wang J, Jenne R, Joseph D (1996) The NCEP/NCAR 40-year reanalysis project. Bull Am Meteorol Soc 77:437–470

Lancelot C, Mathot S, Veth C, de Baar H (1993) Factors controlling phytoplankton ice-edge blooms in the marginal ice-zone of the northwestern Weddell Sea during sea ice retreat 1988: field observations and mathematical modelling. Polar Biol 13:377–387

Lannuzel D, Schoemann V, de Jong J, Tison J-L, Chou L (2007) Distribution and biogeochemical behaviour of iron in the East Antarctic sea ice. Mar Chem 106:18–32

Lavoie D, Denman K, Michel C (2005) Modeling ice algal growth and decline in a seasonally ice-covered region of the Arctic (Resolute Passage, Canadian Archipelago). J Geophys Res 110:C11009. doi:10.1029/2005JC002922

Legendre L, Ackley SF, Dieckmann GS, Gulliksen B, Horner R, Hoshiai T, Melnikov IA, Reeburgh WS, Spindler M, Sullivan CW (1992) Ecology of sea ice biota. 2: Global significance. Polar Biol 12:429–444

Lizotte MP (2001) The contributions of sea ice algae to Antarctic marine primary production. Am Zool 41:57–73

Markus T, Cavalieri DJ (1998) Snow depth distribution over sea ice in the Southern Ocean from passive microwave data. In: Jeffries MO (ed) Antarctic sea ice: physical processes, interactions and variability, vol 74. American Geophysical Union, Washington, DC, pp 19–39

Markus T, Cavalieri DJ (2006) Interannual and regional variability of Southern Ocean snow on sea ice. Ann Glaciol 44:53–57

Massom RA, Eicken H, Haas C, Jeffries MO, Drinkwater MR, Sturm M, Worby AP, Wu X, Lytle VI, Ushio S, Morris K, Reid PA, Warren SG, Allison I (2001) Snow on Antarctic sea ice. Rev Geophys 39:413–445

McMinn A, Ryan KG, Ralph PJ, Pankowski A (2007) Spring sea ice photosynthesis, primary productivity and biomass distribution in eastern Antarctica, 2002–2004. Mar Biol 151:985–995

Monaghan AJ, Bromwich DH, Schneider DP (2008) Twentieth century Antarctic air temperature and snowfall simulations by IPCC climate models. Geophys Res Lett 35:L07502. doi:10.1029/2007GL032630

Nicol S (2006) Krill, currents, and sea ice: *Euphausia superba* and its changing environment. Bioscience 56:111–120

Nicol S, Pauly T, Bindoff NL, Wright S, Thiele D, Hosie GW, Strutton PG, Woehler EJ (2000) Ocean circulation off east Antarctica affects ecosystem structure and sea-ice extent. Nature 406:504–507

Orsi A, Whitworth TIII, Nowlin WD Jr (1995) On the meridional extent and fronts of the Antarctic Circumpolar Current. Deep Sea Res Part I Oceanogr Res Pap 42:641–673

Palmisano AC, SooHoo JB, Moe RL, Sullivan CW (1987) Sea ice microbial communities, VII: changes in under-ice spectral irradiance during the development of Antarctic sea ice microalgal communities. Mar Ecol Prog Ser 35:165–173

Parkinson CL (2002) Trends in the length of the Southern Ocean sea-ice season, 1979–99. Ann Glaciol 34:435–440

Parkinson CL (2004) Southern Ocean sea ice and its wider linkages: insights revealed from models and observations. Antarct Sci 16:387–400

Perovich DK (1996) The optical properties of sea ice. US Army Corps of Engineers, Hanover

Powell DC, Markus T, Stössel A (2005) Effects of snow depth forcing on Southern Ocean sea ice simulations. J Geophys Res 110:C06001. doi:10.1029/2003JC002212

Rintoul SR, Sokolov S, Massom RA (2008) Rapid development and persistence of a massive Antarctic sea ice tongue. J Geophys Res 113:C07045. doi:10.1029/2007JC004541

Sedwick PN, DiTullio GR (1997) Regulation of algal blooms in Antarctic shelf waters by the release of iron from melting sea ice. Geophys Res Lett 24:2515–2518

Siegel V (2005) Distribution and population dynamics of *Euphausia superba*: summary of recent findings. Polar Biol 29:1–22

Siegel V, Loeb V (1995) Recruitment of Antarctic krill *Euphausia superba* and possible causes for its variability. Mar Ecol Prog Ser 123:45–56

Smith WO Jr, Comiso JC (2008) Influence of sea ice on primary production in the Southern Ocean: a satellite perspective. J Geophys Res 113:C05S93. doi:10.1029/2007JC004251

Smith WO Jr, Nelson DM (1985) Phytoplankton bloom produced by a receding ice edge in the Ross Sea: spatial coherence with the density field. Science 227:163–166

Stretch JJ, Hamner PP, Hamner WM, Michel WC, Cook J, Sullivan CW (1988) Foraging behaviour of Antarctic krill *Euphausia superba* on sea ice microalgae. Mar Ecol Prog Ser 44:131–139

Swadling KM (2001) Population structure of two Antarctic ice-associated copepods, *Drescheriella glacialis* and *Paralabidocera antarctica*, in winter sea ice. Mar Biol 139:597–603

Thomas DN, Dieckmann GS (eds) (2003) Sea ice. An introduction to its physics, chemistry, biology and geology. Blackwell Publishing, Oxford, 416 pp

Thorpe SE, Murphy EJ, Watkins JL (2007) Circumpolar connections between Antarctic krill (*Euphausia superba* Dana) populations: investigating the roles of ocean and sea ice transport. Deep Sea Res Part I Oceanogr Res Pap 54:792–810

Trevena AJ, Jones GB (2006) Dimethylsulphide and dimethylsulphoniopropionate in Antarctic sea ice and their release during sea ice melting. Mar Chem 98:210–222

Watanabe K, Satoh H, Takahashi E, Kanda H (1990) Pigment data of sea ice cores collected from fast ice area near Syowa Station, Antarctica, from March 1983 to January 1984(JREA-24). JARE Data Reports 157. Mar Biol 16:1–88

Watterson IG, Dix MR (2003) Simulated changes due to global warming in daily precipitation means and extremes and their interpretation using the gamma distribution. J Geophys Res 108:4379. doi:4310.1029/2002JD002928

Worby AP, Massom RA, Allison I, Lytle VI, Heil P (1998) East Antarctic sea ice: a review of its structure, properties and drift. In: Jeffries MO (ed) Antarctic sea ice: physical processes, interactions, and variability, vol 74. American Geophysical Union, Washington, DC, pp 41–67

Worby AP, Geiger CA, Paget MJ, Van Woert ML, Ackley SF, DeLiberty TL (2008a) Thickness distribution of Antarctic sea ice. J Geophys Res 113:C05S92. doi:10.1029/2007JC004254

Worby AP, Markus T, Steer AD, Lytle VI, Massom RA (2008b) Evaluation of AMSR-E snow depth product over East Antarctic sea ice using in situ measurements and aerial photography. J Geophys Res 113:C05S94. doi:10.1029/2007JC004181

Wright SW, van den Enden RL (2000) Phytoplankton community structure and stocks in the East Antarctic marginal ice zone (BROKE survey, Jan–Mar 1996) determined by CHEMTAX analysis of HPLC pigment signatures. Deep Sea Res Part II Top Stud Oceanogr 47:2363–2400

Zwally HJ, Comiso JC, Parkinson CL, Cavalieri DJ, Gloersen P (2002) Variability of Antarctic sea ice 1979–1998. J Geophys Res 107:3041. doi:3010.1029/2000JC000733